Geophysical Research Letters

RESEARCH LETTER
10.1029/2022GL100175

Key Points:

- Longwave adjustments from the stratosphere warmed by wildfire smoke are comparable to shortwave radiative forcing
- The simulated annual mean effective RF (ERF) from the Australian wildfire is −0.17, −0.22, and −0.37 W/m^2 at the top of the atmosphere, 200 hPa, and the surface
- The simulated ERF of stratospheric wildfire smoke is 70%–270% more negative than the mass-equivalent sulfate in the CESM-MAM3 model

Supporting Information:

Supporting Information may be found in the online version of this article.

Correspondence to:

S. Liu and P. Yu,
shangliu2012@gmail.com;
pengfei.yu@colorado.edu

Citation:

Liu, C.-C., Portmann, R. W., Liu, S., Rosenlof, K. H., Peng, Y., & Yu, P. (2022). Significant effective radiative forcing of stratospheric wildfire smoke. *Geophysical Research Letters*, *49*, e2022GL100175. https://doi.org/10.1029/2022GL100175

Received 24 JUN 2022
Accepted 25 AUG 2022

Author Contributions:

Conceptualization: Pengfei Yu
Data curation: Cheng-Cheng Liu, Pengfei Yu
Formal analysis: Cheng-Cheng Liu
Funding acquisition: Pengfei Yu
Investigation: Cheng-Cheng Liu
Methodology: Cheng-Cheng Liu, Yifeng Peng, Pengfei Yu
Project Administration: Pengfei Yu
Resources: Pengfei Yu
Supervision: Shang Liu, Pengfei Yu
Validation: Robert W. Portmann, Pengfei Yu
Visualization: Cheng-Cheng Liu
Writing – original draft: Cheng-Cheng Liu

Significant Effective Radiative Forcing of Stratospheric Wildfire Smoke

Cheng-Cheng Liu[1], Robert W. Portmann[2], Shang Liu[1,3], Karen H. Rosenlof[2], Yifeng Peng[4], and Pengfei Yu[5]

[1]School of Earth and Space Sciences, University of Science and Technology of China, Hefei, China, [2]Chemical Science Laboratory, National Oceanic and Atmospheric Administration, Boulder, CO, USA, [3]Now at Research Division, California Air Resources Board, Sacramento, CA, USA, [4]College of Atmospheric Sciences, Lanzhou University, Lanzhou, China, [5]Institute for Environmental and Climate Research, Jinan University, Guangzhou, China

Abstract The radiative forcing (RF) of volcanic sulfate is well quantified. However, the RF of pyrocumulonimbus (pyroCb) smoke with absorbing carbonaceous aerosols has not been considered in climate assessment reports. With the Community Earth System Model, we studied two record-breaking wildfire events, the 2017 Pacific Northwest Event (PNE) and the 2019–2020 Australian New Year event (ANY), that perturbed stratospheric chemistry and the earth's radiation budget. We calculated a global annual-mean effective RF (ERF) of -0.04 ± 0.02 and -0.17 ± 0.02 W/m^2 at the top of the atmosphere (TOA) for PNE and ANY, respectively. The complexity of longwave RF led to an uncertainty of about 50% in the ERF at the TOA among climate models. We found that modeled ERF from wildfire smoke was 70%–270% more negative than the ERF of mass-equivalent sulfate aerosol, highlighting its important role in the climate radiative budget.

Plain Language Summary Extreme wildfires can directly inject a large amount of smoke into the stratosphere. Two recent record-breaking wildfire events influenced stratospheric chemistry and the global climate. However, the climate effects of these wildfires remain relatively unclear comparing to those of well-known volcanic eruptions. We used a climate model to simulate the global effective radiative effects. Results show that the wildfire smokes significantly cooled the Earth system, with -0.04 ± 0.02 and -0.17 ± 0.02 W/m^2 for each fire. Longwave radiation from the stratosphere warmed by the wildfire smoke was comparable to shortwave radiative forcing. We further compared the climate effects of smoke to volcanic sulfate with the same aerosol mass injected. We found that wildfire smoke can cool the atmosphere 70%–270% more effectively than sulfate aerosol.

1. Introduction

The pyrocumulonimbus (pyroCb) induced by extreme wildfires can inject many smoke particles into the stratosphere (Fromm et al., 2005, 2010; Peterson et al., 2018). The stratospheric lifetime of smoke particles ranges from months to years (D'Angelo et al., 2022; Das et al., 2021; Kremser et al., 2016; Yu et al., 2019) depending on the season and latitude of injection. The upwelling tropical air prolongs the stratospheric lifetime of the injected aerosols. In contrast, particles injected at the mid-high latitudes are subject to more rapid removal (Deshler, 2008; Trickl et al., 2013). This long-lasting smoke can perturb stratospheric chemistry and the aerosol budget. The smoke particles primarily consist of organic matter (OM), with minor black carbon (BC). The estimated mass fraction of BC is about 2%–3% calculated by constraining model simulations with satellite observations (Yu et al., 2019, 2021). A similar BC mass fraction was observed by in situ measurements during the Atmospheric Tomography Mission (Ditas et al., 2018; Froyd et al., 2019). Since the frequency of pyroCb events may increase in a warming climate (Di Virgilio et al., 2019; Peterson et al., 2021), a comprehensive investigation of the radiative effects of pyroCb events is needed in climate evaluation and prediction.

Two record-breaking pyroCb events in the last decade injected large amounts of aerosols into the stratosphere. The 2017 Pacific Northwest Event (PNE) injected about 0.3 Tg (0.1–0.35 Tg) smoke (S. M. Khaykin et al., 2018; Peterson et al., 2018; Torres et al., 2020; Yu et al., 2019) with plumes lofting from 12 to 23 km (Ansmann et al., 2018; Baars et al., 2019). The 2019–2020 Australian New Year wildfire event (ANY) injected about 3 times the mass (0.3–2.1 Tg) of the 2017 PNE (Hirsch & Koren, 2021; Kablick et al., 2020; S. Khaykin et al., 2020; Peterson et al., 2021; Yu et al., 2021). This smoke mass is comparable to the injection of SO_2 from a moderate

Writing – review & editing: Cheng-Cheng Liu, Robert W. Portmann, Shang Liu, Karen H. Rosenlof, Pengfei Yu

volcanic eruption (Peterson et al., 2018, 2021). Recent observational and modeling studies have found that the 2019–2020 ANY event warmed the stratosphere by 1–2 K (Rieger et al., 2021; Yu et al., 2021) and depleted the stratospheric ozone by a few percent through heterogeneous chemistry (Bernath et al., 2022; Santee et al., 2022; Solomon et al., 2022; Yu et al., 2021).

Radiative forcing (RF) denotes an imbalance of the radiation budget induced by various forcing agents including aerosols and trace gases. Quantification of RF can evaluate the climate impacts of stratospheric injections of aerosols including volcanic eruptions and pyroCb events (Bellouin et al., 2020). The RF of volcanic eruptions is relatively well quantified. For example, the 1991 Pinatubo eruption with 10–18 Tg SO_2 (Mills et al., 2016) induced a global peak RF of -3.2 W/m^2 and an annual-mean RF of more than -2.09 W/m^2 in 1992 (G. A. Schmidt et al., 2014; A. Schmidt et al., 2018). The decadal average RF of small to moderate volcanic eruptions is estimated to be between -0.1 and -0.2 W/m^2 (Brühl et al., 2015; Ridley et al., 2014; A. Schmidt et al., 2018; Solomon et al., 2011). Volcanic sulfate aerosols cool the Earth by scattering sunlight back to space with minor absorption of terrestrial longwave radiation. However, the wildfire smoke particles not only scatter sunlight but also absorb sunlight and heat the stratosphere in the shortwave. Furthermore, the longwave radiation from the warmed stratosphere complicates their total RF estimation. In general, the RF of pyroCb events remains less understood compared to volcanic emissions (Peterson et al., 2018). For the 2017 PNE, Christian et al. (2019) modeled a slightly positive global instantaneous RF of about 0.02 W/m^2 at the top of the atmosphere (TOA). Das et al. (2021) reported global all-sky RF at the TOA and surface of -0.03 ± 0.01 and -0.12 ± 0.03 W/m^2, respectively. For the 2019–2020 ANY, Yu et al. (2021) suggested a negative global clear-sky effective RF (ERF) of -0.03 W/m^2 at the TOA and -0.32 W/m^2 at the surface. Using measured aerosol optical properties, S. Khaykin et al. (2020) computed peak shortwave RF values of -0.31 ± 0.09 W/m^2 at the TOA and -0.98 ± 0.17 W/m^2 at the surface in February 2020. Similarly, Sellitto et al. (2022) estimated -0.35 ± 0.21 and -0.94 ± 0.26 W/m^2 at the TOA and surface in February. Based on satellite measurements, Hirsch and Koren (2021) estimated a cooling shortwave RF at TOA of -1.0 ± 0.6 W/m^2 in January, which decayed to -0.5 ± 0.4 W/m^2 in June. Nevertheless, the longwave RF of the smoke-warmed stratosphere has not been well quantified.

In this study, we quantified the climate-relevant ERF of the two largest pyroCb events (PNE and ANY) at the TOA, 200 hPa, and the surface in the last decade using the Community Earth System Model (CESM). We further compared the simulated ERF of smoke and sulfate aerosols with the same mass of materials injected. We show that the wildfire smoke can cool the atmosphere 70%–270% more effectively than mass-equivalent sulfate in the model.

2. Methods

2.1. CESM-MAM3

The CESM1.2.2 model coupled with an atmospheric component of the Community Atmosphere Model version 5 (CAM5) was used for our simulation (Lamarque et al., 2012). The interactive aerosol chemistry was represented by a Modal Aerosol Module (Liu et al., 2012) with three lognormal modes (MAM3). Using the prognostic aerosol optical properties from MAM3, the Rapid Radiative Transfer Model for Global Climate Models (RRTMG) was applied to simulate the radiative flux for both shortwave and longwave (Iacono et al., 2008; Mlawer et al., 1997). Detailed model configurations are provided in Text S1 in Supporting Information S1.

We conducted three sets of ensemble experiments to simulate pyroCb smoke and volcanic sulfate. Each set contained 60-member ensembles (free-run) from MAM3 (Text S1 in Supporting Information S1). (a) The control experiment without stratospheric pyroCb smoke or volcanic sulfate; (b) The pyroCb experiment with the smoke inventory listed in Table S1 in Supporting Information S1; (c) The pyroCb-equivalent volcanic experiment that injected the same mass of sulfate as the smoke mass injected in set (b). In the volcanic experiment, we injected sulfate at 18 km in the stratosphere. To validate these results, we conducted extra experiments with 20 ensembles from the Community Aerosol and Radiation Model for Atmospheres (CARMA) (Yu et al., 2021).

2.2. Satellite Observations

We used aerosol extinction coefficient products from two satellites to validate our model simulations, that is, the Ozone Mapping and Profiler Suite Limb Profiler (OMPS-LP) (Loughman et al., 2018) and the Stratospheric

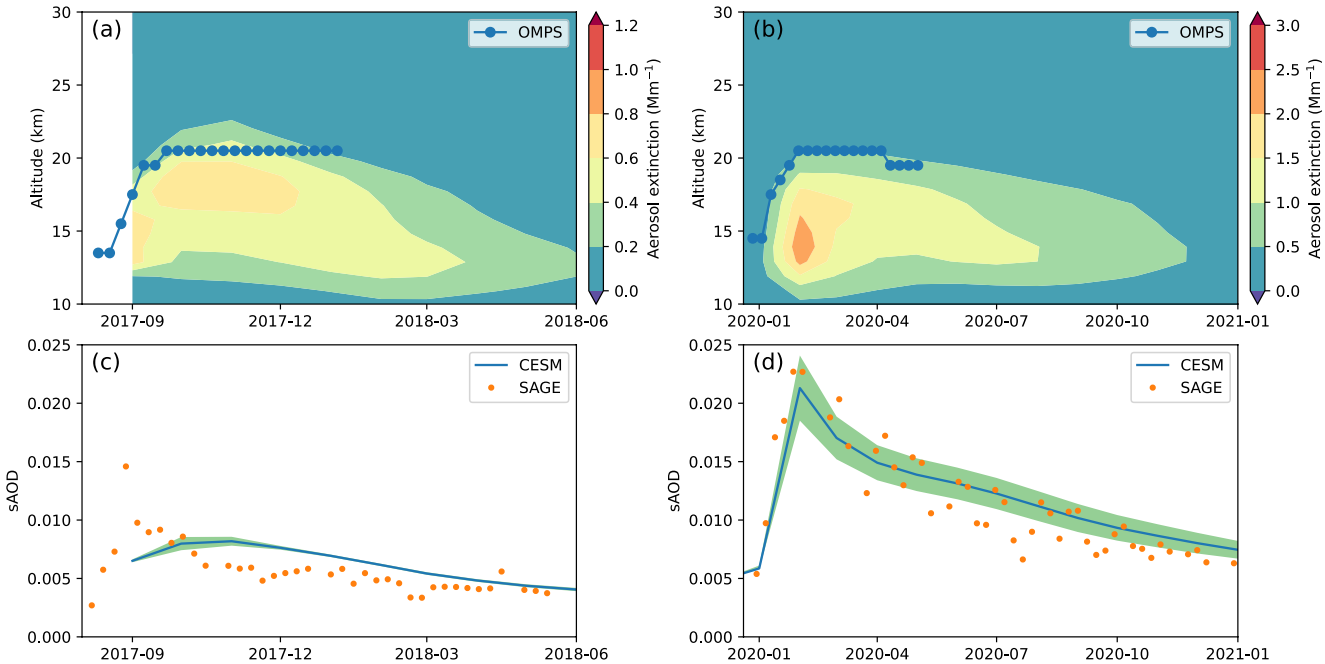

Figure 1. (a) Comparison between the simulated vertical distributions of the aerosol extinction coefficient over 20–60°N (contour map) and observations by Ozone Mapping and Profiler Suite Limb Profiler (OMPS-LP) for Pacific Northwest Event (PNE). The solid blue line with filled circles denotes the plume maximum height derived from OMPS-LP. The maximum height is defined as the highest altitude where the horizontal-mean extinction at 675 nm is greater than 0.3 and 0.5 Mm^{-1} for PNE and Australian New Year event (ANY), respectively. (b) Same as (a) but for ANY over 20–60°S; (c) Comparison between simulated stratospheric aerosol optical depth (sAOD) integrated from 12 to 30 km and observations by SAGE III/ISS for PNE. The green shading denotes standard deviation of the model ensembles. (d) Same as (c) but for ANY.

Aerosol and Gas Experiment III on the International Space Station (SAGE III/ISS) (Chen et al., 2020). Details are provided in Text S2 in Supporting Information S1.

3. Results and Discussion

3.1. Smoke Distribution

As shown in Figure 1, the smoke plume ascended from 12 to 15 km to over 20 km within 1–2 months and slowly descended in the following months. The observed and modeled mid-latitude stratospheric aerosol optical depth (sAOD) from 12 to 30 km was enhanced by a factor of 1 and 3.5 by the 2017 PNE and 2019–2020 ANY events, respectively. The sAOD enhancements remained in the stratosphere for >6 months for PNE and up to 1 year for ANY. The observed mid-latitude aerosol extinction coefficients at 12.5, 15.5, 18.5, and 21.5 km are shown in Figure S1 in Supporting Information S1. Both observations and model simulations suggest that the aerosol extinction coefficients at 21.5 km peaked about 1 month later than those at 15.5 km. The delayed peak at the higher altitude is associated with the rising plume.

3.2. Stratospheric Warming

Satellite observations (Bernath et al., 2022; Rieger et al., 2021; Santee et al., 2022) showed that the 2019–2020 ANY smoke warmed the lower stratosphere of the mid-latitudes in the Southern Hemisphere (SH) by 1–2 K for 6 months and peaked at about 2.5 K in February 2020 (Santee et al., 2022) (Figure S2 in Supporting Information S1). Model simulations suggest that the stratospheric warming is mostly due to the shortwave absorption of smoke (Yu et al., 2021). Here we simulated the global mean stratospheric temperature anomalies from 10 to 30 km between 2017 and 2021 (Figure 2). Simulated stratospheric warming due to ANY was over 1 K for the global mean temperature (Figure 2) and over 1.5 K averaged in the SH mid-latitudes (Figure S2 in Supporting Information S1). Simulated global mean temperature anomalies greater than 0.4 K persisted throughout 2021. As the plume rose in the first 3 months, the simulated maximum height of the smoke rose from 12 to 23 km.

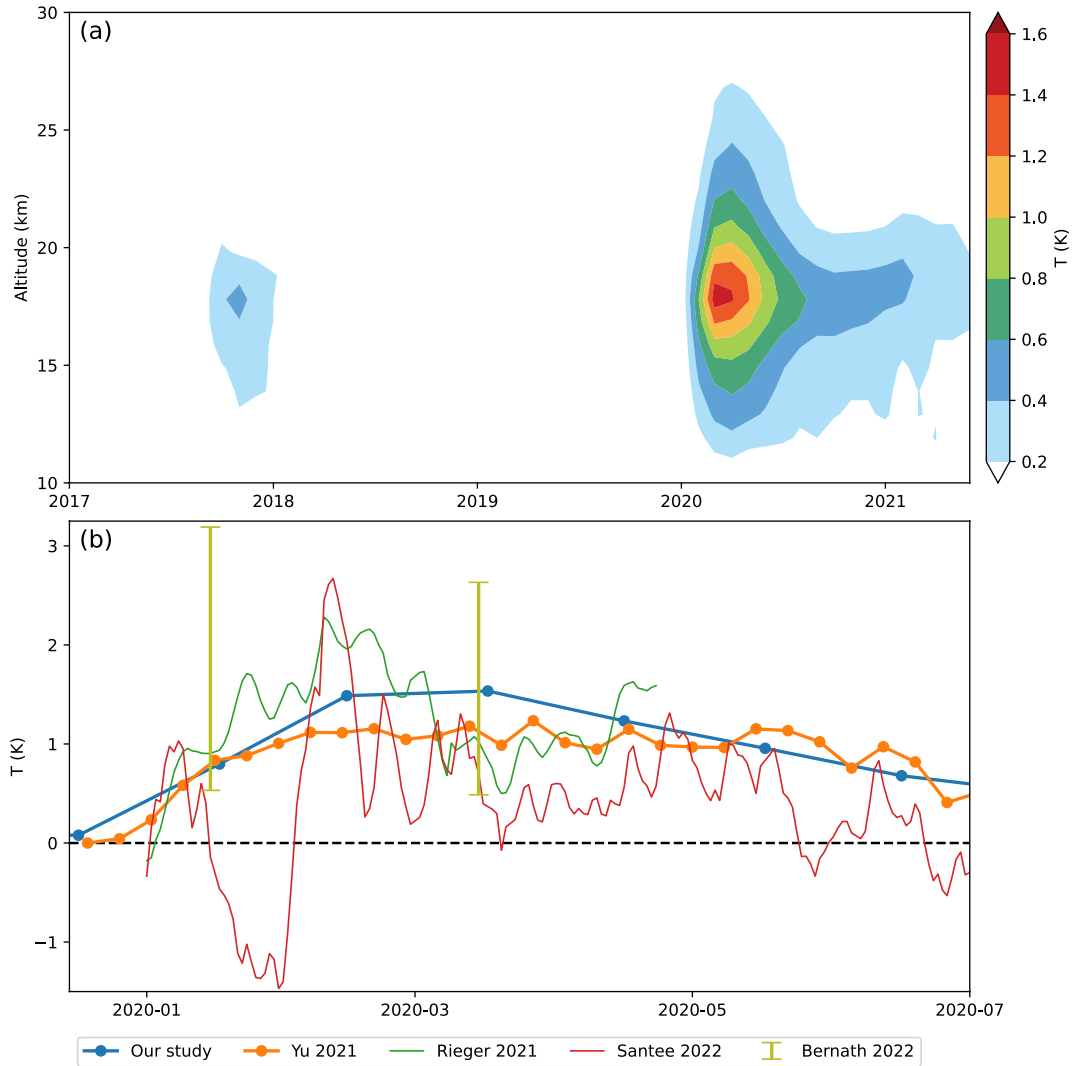

Figure 2. (a) Simulated vertical distributions of the global mean temperature anomalies for the 2017 Pacific Northwest Event (PNE) and the 2019–2020 Australian New Year event (ANY) events. (b) Comparison of the simulated temperature anomalies due to ANY with satellite observations. The temperature anomalies from Yu et al. (2021), Rieger et al. (2021), and the current study are averaged between 30°S and 60°S. The temperature anomalies reported in Santee et al. (2022) are relative to the averaged temperature from 2005 to 2019 at 480 K (about 19 km) between 38°S and 54°S. Bernath et al. (2022) reported the temperature anomalies relative to 2005–2019 from 45°S to 60°S. The error bar represents the minimum to maximum anomalies for January and March 2020.

The peak warming remained below 20 km where the main smoke plume was located. In contrast, the 2017 PNE induced a weaker global stratospheric warming of 0.2–0.6 K, which lasted about 4 months (Stocker et al., 2021). The warming from PNE was weaker mainly because the smoke injected by PNE was about 70% less than ANY.

In Figure 2b, we compare the observed and simulated stratospheric warming for the 2019–2020 ANY over the SH. In general, both the satellite observations (Bernath et al., 2022; Rieger et al., 2021; Santee et al., 2022) and model simulations by MAM3 (the present study) and CARMA (Yu et al., 2021) show that the SH mid-latitude stratosphere was warmed by about 1–2 K for a few months. The peak warming simulated by MAM3 was 0.5 K higher than that simulated by CARMA because the shortwave absorption of smoke organics was considered in MAM3 but ignored in CARMA (Table S2 in Supporting Information S1).

The smoke aerosols of the 2019–2020 ANY are composed of 2.5% BC and 97.5% OM according to a modeling study (Yu et al., 2021). To evaluate the relative contribution of OM and BC to the stratospheric warming, we conducted two sensitivity tests with the same smoke mass but containing 10% and 0% BC, respectively. The

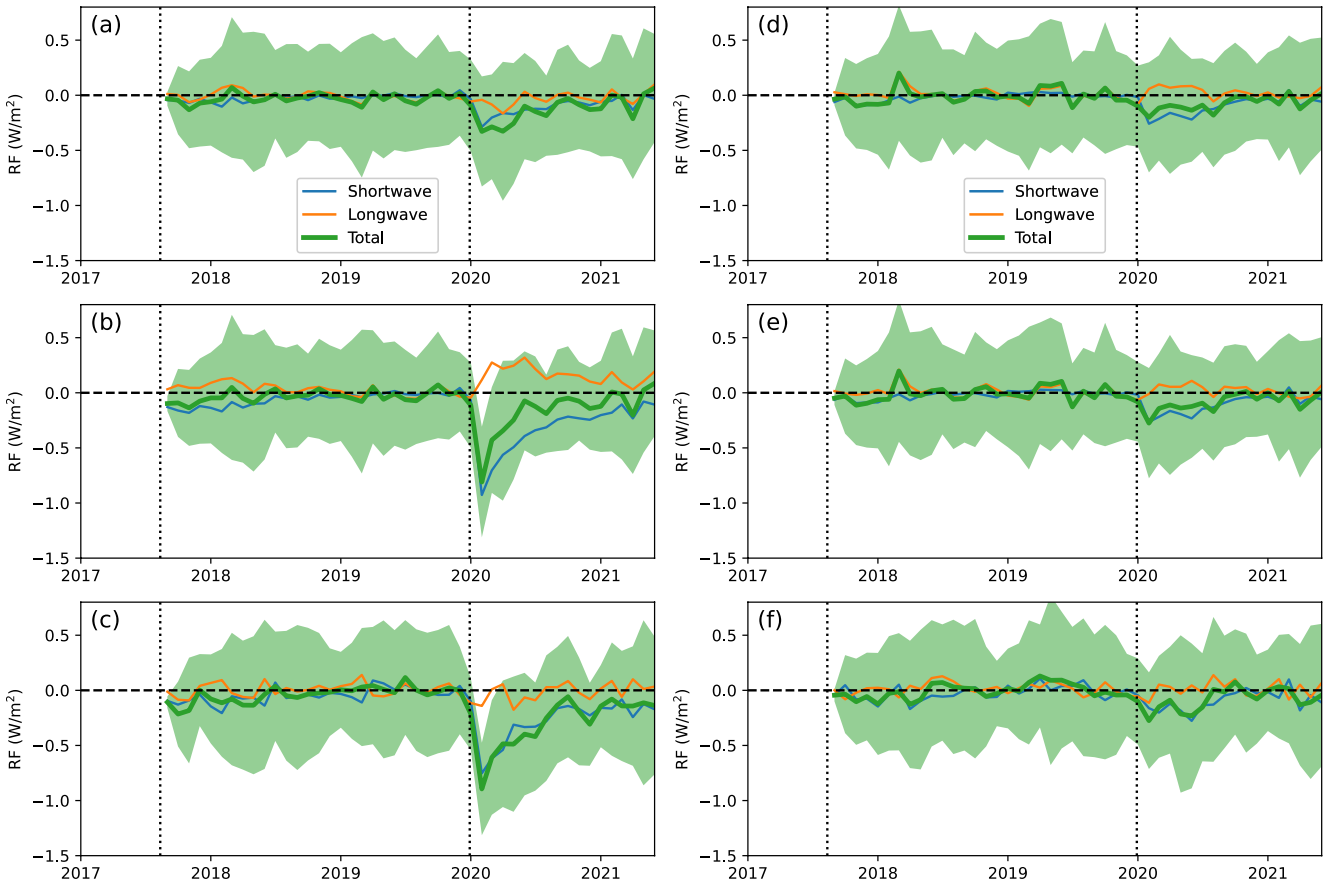

Figure 3. Global-mean (60°N − 60°S) clear-sky ERF of pyroCb at (a) the top of the atmosphere (TOA), (b) 200 hPa, and (c) the surface. Panels (d–f) are the same as (a–c) but for the simulated ERF with the mass-equivalent sulfate injected at 18 km. The refractive index (RI) at 550 nm of smoke organic matter (OM) and sulfate aerosols in MAM3 is 1.53 + 0.0057i and 1.43 + 10^{-8}i (Table S2 in Supporting Information S1). Blue lines denote shortwave ERF. Orange lines denote longwave ERF. Green lines denote total ERF (shortwave + longwave). Shading denotes one standard deviation of 60-member ensemble runs from MAM3. Vertical dotted lines denote the injection time of the 2017 Pacific Northwest Event (PNE) and 2019–2020 Australian New Year event (ANY) events.

10%-BC case showed stronger warming for the two pyroCb events at higher altitude (up to 28 km). The 0%-BC experiment suggested about 0.5 K temperature variations in 4 months (about 1/3–1/4 the temperature enhancement of the 2.5%-BC experiment used as the result) for the 2019–2020 ANY (Figure S3 in Supporting Information S1). With an offline Mie code, we found that the calculated absorption coefficient from OM in the smoke was comparable to that from BC at 550 nm with the refractive index (RI) used in MAM3 (Table S3 in Supporting Information S1). Our study suggests that both BC and the absorbing OM in the smoke in MAM3 contributed significantly to stratospheric warming.

3.3. Effective Radiative Forcing

Stratospheric absorbing aerosols (e.g., BC and absorbing OM) warm the stratosphere but cool the surface (Ban-Weiss et al., 2012). The rapid adjustment of longwave radiation balances the shortwave radiation anomaly by smoke absorption. The ERF, a climate-relevant metric that considers rapid stratospheric adjustment (Larson & Portmann, 2016), was calculated to quantify the radiative impacts of pyroCb events. In this study, we define downward ERF as positive for both shortwave and longwave radiation. Thus, positive ERF values represent warming of the Earth system. We report the global mean ERF values averaged from 60°N to 60°S to avoid the simulated dynamically driven variability in the polar regions.

Statistically significant global mean clear-sky ERF was found in late 2017 and 2020 associated with the two major pyroCb events (Figure 3). For the 2017 PNE, the simulated global mean ERF reached a minimum of less than −0.2 W/m^2 within the first 2–3 months and decayed to zero by the end of 2017. In contrast, the ERF from the

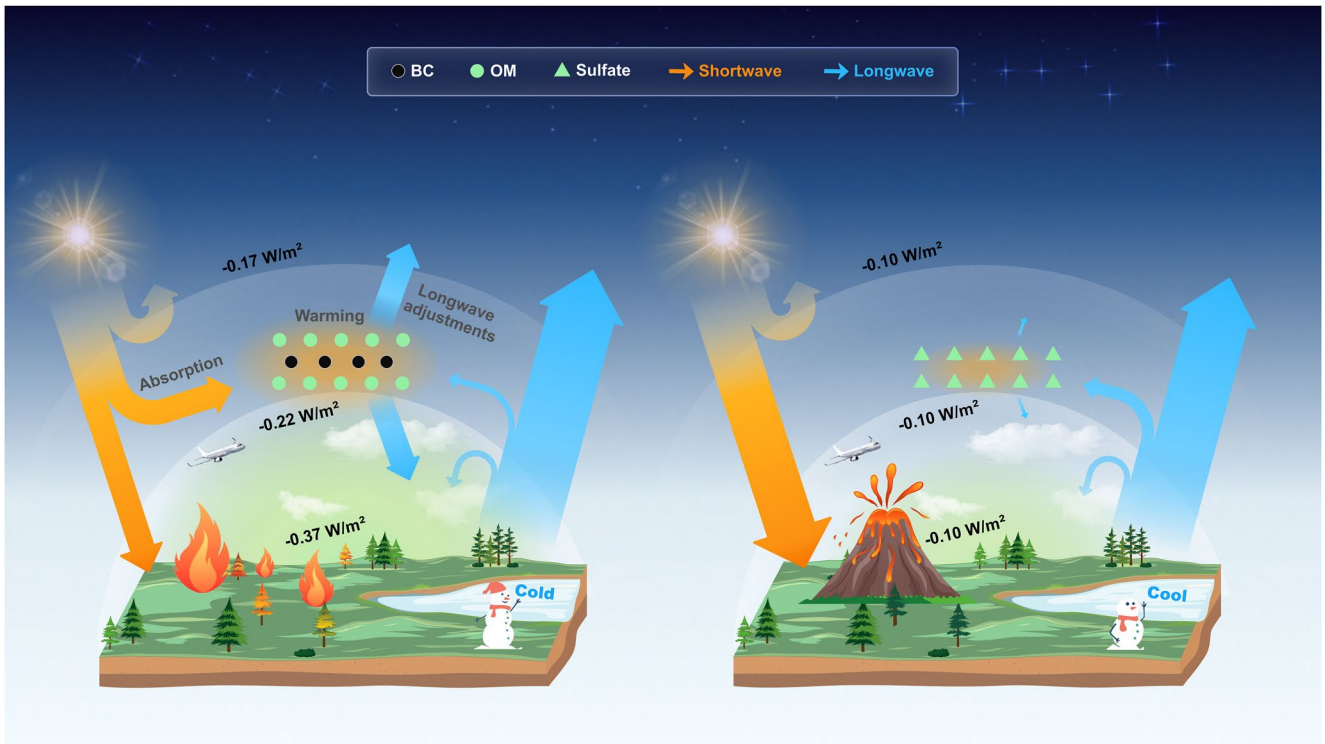

Figure 4. Schematic diagram for the ERF of pyroCb smoke (left) and volcanic sulfate (right). The orange arrows indicate shortwave radiation, and the blue arrows denote longwave radiation. Black carbon (BC), organic matter (OM), and sulfate aerosols are denoted by different symbols. The numbers represent simulated annual-mean ERF at the top of the atmosphere (TOA), 200 hPa, and the surface for ANY smoke and mass-equivalent sulfate. The detailed ERF values are presented in Tables S4 and S6 in Supporting Information S1.

2019–2020 ANY event reached a minimum of about −0.4 W/m^2 at the TOA and at about −0.8 W/m^2 at 200 hPa and the surface. The simulated ERF of the ANY event lasted for more than 6 months in a broader latitudinal range of 10–60°S (Figure S4 in Supporting Information S1). As shown in Table S4 in Supporting Information S1, the simulated global mean ERF values for ANY are −0.17, −0.22, and −0.37 W/m^2 from the TOA, 200 hPa, and the surface, respectively. These values are about 4 times those of the 2017 PNE event in the first year.

The total ERF (shortwave + longwave) was dominated by the incoming shortwave RF, with rapid adjustment from the longwave RF (Figure 4). The simulated shortwave RF at the surface was significantly larger than the value at the TOA because the stratospheric smoke absorbed considerable incoming solar energy and persistently warmed the stratosphere (Yu et al., 2021). Consequently, less downward shortwave radiation reached 200 hPa and the surface. The warming stratosphere emitted more longwave RF both up to the TOA and down to 200 hPa compared to the smoke-free condition. The simulated longwave RF due to the ANY event was −0.04 ± 0.02 and 0.17 ± 0.02 W/m^2 at the TOA and 200 hPa, respectively. At 200 hPa, the magnitude of the simulated longwave RF was about 50% of the shortwave RF (Figure 3 and Table S4 in Supporting Information S1). Our model simulations suggest that pyroCb smoke significantly warmed the stratosphere but had a cooling influence on the troposphere and surface (Figure 4).

The stratospheric smoke induced a convergence of energy in the first few months and then adjusted back to equilibrium by longwave RF. As shown in Figure S5a in Supporting Information S1, the total RF at 200 hPa was about 80%–200% more negative than the TOA RF for 1–3 months. Subsequently, the combined effects of shortwave and longwave RF resulted in comparable ERF at 200 hPa and TOA, although the shortwave RF is considerably more negative at 200 hPa compared to TOA. We further found a delayed peak time of 1–3 months in longwave ERF compared to shortwave ERF at the TOA and 200 hPa (Figure 3). This is consistent with the simulated temperature anomalies shown in Figure 2. The simulated delayed longwave ERF resulted from stratospheric temperature adjustments (Smith et al., 2018) in response to the absorbing smoke.

The complexity between MAM3 and CARMA for longwave RF led to an uncertainty of about 50% for ERF at the TOA, despite the overall consistency otherwise. MAM3 modeled more negative longwave RF at the TOA

compared to CARMA (Yu et al., 2021) from January to June 2020 (Figure S5 in Supporting Information S1). In contrast, CARMA simulated a positive longwave RF of 0.04 ± 0.04 W/m^2, which offset the negative shortwave RF at the TOA (Table S4 in Supporting Information S1). MAM3 introduced more longwave cooling partly because it generated more stratospheric warming from smoke organics than CARMA (Figure 2). Li et al. (2021) suggested that the organics RI and mixing state could contribute to ±100% simulation uncertainties for the shortwave RF. Here we further complement the large diversity in longwave adjustments for ERF among climate models. Since the real part of the organics RI usually varies from 1.3 to 1.65 and the imaginary part from 0i to 0.02i (Bond & Bergstrom, 2006; Saleh et al., 2014), such variability makes longwave radiation more complicated and difficult to quantify. Besides the RI, the aerosol microphysical properties (e.g., size distributions and mixing state) can affect simulated aerosol burden and lifetime. Our results suggest that better representations of the optical and microphysical properties of smoke aerosols in the models could improve the evaluation of climate responses from pyroCb.

3.4. Comparison of Smoke Aerosols and Sulfate

The ERF of the 2017 PNE and the 2019–2020 ANY events calculated in this study is comparable to the reported ERF of moderate volcanic eruptions (G. A. Schmidt et al., 2014; A. Schmidt et al., 2018) (Table S5 in Supporting Information S1). The simulated ERF per mass injected is −0.13 and −0.19 W m^{-2} Tg^{-1} for PNE and ANY, respectively. The calculated ERF per unit mass injected for SO_2 for the Kasatochi, Sarychev, and Nabro eruptions from 2008 to 2011 is smaller by a factor of about 1–2 than for the two pyroCb events. This comparison suggests that small emissions by wildfires may produce disproportionally larger climate effects than volcanos. However, the injection time, latitude, and altitude vary among the pyroCb and volcanic events, which makes it difficult to compare their ERF per mass directly. Furthermore, to understand the microphysical mechanisms that resulted in the ERF differences between the wildfire and volcanic emissions, we conducted "idealized" volcanic experiments that replaced the smoke aerosols with the same amount of sulfate injected (see Section 2).

As shown in Figure 3, the simulated annual-mean ERF for ANY smoke was over 1.7 times that of the idealized volcanic events. Consistently, the simulated sAOD anomaly of smoke at 675 nm was 70% higher than that of sulfate (Figure S6 in Supporting Information S1). This can be explained by the different RI between organics and sulfate in MAM3. Our offline Mie calculation confirmed that the higher real and imaginary parts of RI for BC and OM produced 70% higher aerosol extinction than sulfate aerosol at 550 nm (Table S3 in Supporting Information S1). As shown in Figure 4, the shortwave ERF at the TOA was similar in magnitude between smoke and sulfate; however, the negative longwave adjustment of smoke from stratospheric warming contributed to a larger TOA ERF. At 200 hPa and the surface, the pyroCb smoke produced a negative ERF that was a factor of 2.2–3.7 to volcanic sulfate (Table S6 in Supporting Information S1). This is because the stratospheric smoke absorbed a portion of the shortwave radiation, which arrived at 200 hPa and the surface in the idealized volcanic case (Figure 4). Another set of 20-member ensemble runs by CESM-CARMA also produced similar ERF for sulfate aerosol with consistent RI as the CESM-MAM3 model (Table S6 in Supporting Information S1).

4. Conclusions

The two record-breaking pyroCb events (the 2017 PNE and the 2019–2020 ANY event) perturbed stratospheric chemistry and the radiative budget. We ran the CESM-MAM3 climate model to quantify the ERF of these two pyroCb events. Both the model and satellite observations show that sAOD was enhanced by a factor of about 1 and three in the first 2 months of the PNE and ANY event, respectively. The plumes from the two pyroCb events self-lofted from 12 km to over 21 km in the first 3 months due to shortwave absorption by the smoke particles (de Laat et al., 2012). Consistent with satellite observations, we found that the ANY smoke warmed the stratosphere in the Southern Hemisphere midlatitudes by 1–1.5 K from 12 to 22 km for about 6 months. In the CESM-MAM3 model, we found that both the organics and BC components of the smoke contributed to stratospheric warming with similar magnitude.

The simulated annual and global mean clear-sky ERF for the ANY event was −0.17 ± 0.02, −0.22 ± 0.02, and −0.37 ± 0.03 W/m^2 at the TOA, 200 hPa, and the surface, respectively. The simulated ERF of ANY was more negative than that of PNE by a factor of about 3. The stratospheric temperature adjustments from the warming stratosphere partly offset the shortwave cooling at 200 hPa but strengthened the cooling at the TOA. However, the

total ERF at the TOA simulated by the CARMA sectional aerosol model was about 50% lower than that simulated by the CESM-MAM3 model. Our study highlights the importance of longwave adjustments in ERF simulations for absorbing smoke, calling for more robust measurements and representations of the optical and microphysical properties for pyroCb smoke to enhance their climate predictability in the model.

To compare the ERF for wildfire smoke and volcanic sulfate directly, we conducted sensitivity simulations with sulfate injected instead of carbonaceous aerosols. We found that the simulated ERF of smoke was about 70% more negative than that of sulfate at the TOA, and about 120%–270% more negative at 200 hPa and the surface. A schematic diagram summarized the major similarities and differences in the radiative processes between smoke aerosols and sulfate (Figure 4). We found that the difference between the simulated ERF of smoke and sulfate resulted from the different RI used in the model as well as the rapid adjustment in response to stratospheric heating. Our study demonstrated that the stratospheric wildfire smoke significantly perturbed the climate radiative budget, which needs to be evaluated in climate assessments.

Data Availability Statement

Model simulations are publicly available at https://doi.org/10.5281/zenodo.7039968. OMPS-LP data are publicly available at https://ozoneaq.gsfc.nasa.gov/data/ozone/. SAGE III/ISS data are publicly available at https://doi.org/10.5067/ISS/SAGEIII/SOLAR_HDF5_L2-V5.2.

Acknowledgments
This work has been supported by the National Natural Science Foundation of China (42175089, 42121004, 21777151) and the second Tibetan Plateau Scientific Expedition and Research Program (2019QZKK0604). CCL and YP were partly supported by the Guangdong Innovative and Entrepreneurial Research Team Program (2016ZT06N263). We thank the High Performance Computing Public Service Platform of Jinan University. The CESM project is supported by the National Science Foundation and the Office of Science (BER) of the U.S. Department of Energy.

References

Ansmann, A., Baars, H., Chudnovsky, A., Mattis, I., Veselovskii, I., Haarig, M., et al. (2018). Extreme levels of Canadian wildfire smoke in the stratosphere over central Europe on 21–22 August 2017. *Atmospheric Chemistry and Physics*, *18*(16), 11831–11845. https://doi.org/10.5194/acp-18-11831-2018

Baars, H., Ansmann, A., Ohneiser, K., Haarig, M., Engelmann, R., Althausen, D., et al. (2019). The unprecedented 2017–2018 stratospheric smoke event: Decay phase and aerosol properties observed with the EARLINET. *Atmospheric Chemistry and Physics*, *19*(23), 15183–15198. https://doi.org/10.5194/acp-19-15183-2019

Ban-Weiss, G. A., Cao, L., Bala, G., & Caldeira, K. (2012). Dependence of climate forcing and response on the altitude of black carbon aerosols. *Climate Dynamics*, *38*(5), 897–911. https://doi.org/10.1007/s00382-011-1052-y

Bellouin, N., Quaas, J., Gryspeerdt, E., Kinne, S., Stier, P., Watson-Parris, D., et al. (2020). Bounding global aerosol radiative forcing of climate change. *Reviews of Geophysics*, *58*(1), e2019RG000660. https://doi.org/10.1029/2019RG000660

Bernath, P., Boone, C., & Crouse, J. (2022). Wildfire smoke destroys stratospheric ozone. *Science*, *375*(6586), 1292–1295. https://doi.org/10.1126/science.abm5611

Bond, T. C., & Bergstrom, R. W. (2006). Light absorption by carbonaceous particles: An investigative review. *Aerosol Science and Technology*, *40*(1), 27–67. https://doi.org/10.1080/02786820500421521

Brühl, C., Lelieveld, J., Tost, H., Höpfner, M., & Glatthor, N. (2015). Stratospheric sulfur and its implications for radiative forcing simulated by the chemistry climate model EMAC. *Journal of Geophysical Research: Atmospheres*, *120*(5), 2103–2118. https://doi.org/10.1002/2014JD022430

Chen, Z., Bhartia, P. K., Torres, O., Jaross, G., Loughman, R., Deland, M., et al. (2020). Evaluation of the OMPS/LP stratospheric aerosol extinction product using SAGE III/ISS observations. *Atmospheric Measurement Techniques*, *13*(6), 3471–3485. https://doi.org/10.5194/amt-13-3471-2020

Christian, K., Wang, J., Ge, C., Peterson, D., Hyer, E., Yorks, J., & McGill, M. (2019). Radiative forcing and stratospheric warming of pyrocumulonimbus smoke aerosols: First modeling results with multisensor (EPIC, CALIPSO, and CATS) views from space. *Geophysical Research Letters*, *46*(16), 10061–10071. https://doi.org/10.1029/2019GL082360

D'Angelo, G., Guimond, S., Reisner, J., Peterson, D. A., & Dubey, M. (2022). Contrasting stratospheric smoke mass and lifetime from 2017 Canadian and 2019/2020 Australian megafires: Global simulations and satellite observations. *Journal of Geophysical Research: Atmospheres*, *127*(10), e2021JD036249. https://doi.org/10.1029/2021JD036249

Das, S., Colarco, P. R., Oman, L. D., Taha, G., & Torres, O. (2021). The long-term transport and radiative impacts of the 2017 British Columbia pyrocumulonimbus smoke aerosols in the stratosphere. *Atmospheric Chemistry and Physics*, *21*(15), 12069–12090. https://doi.org/10.5194/acp-21-12069-2021

de Laat, A. T. J., Stein Zweers, D. C., Boers, R., & Tuinder, O. N. E. (2012). A solar escalator: Observational evidence of the self-lifting of smoke and aerosols by absorption of solar radiation in the February 2009 Australian Black Saturday plume. *Journal of Geophysical Research*, *117*(D4), D04204. https://doi.org/10.1029/2011jd017016

Deshler, T. (2008). A review of global stratospheric aerosol: Measurements, importance, life cycle, and local stratospheric aerosol. *Atmospheric Research*, *90*(2), 223–232. https://doi.org/10.1016/j.atmosres.2008.03.016

Ditas, J., Ma, N., Zhang, Y., Assmann, D., Neumaier, M., Riede, H., et al. (2018). Strong impact of wildfires on the abundance and aging of black carbon in the lowermost stratosphere. *Proceedings of the National Academy of Sciences*, *115*(50), E11595–E11603. https://doi.org/10.1073/pnas.1806868115

Di Virgilio, G., Evans, J. P., Blake, S. A. P., Armstrong, M., Dowdy, A. J., Sharples, J., & McRae, R. (2019). Climate change increases the potential for extreme wildfires. *Geophysical Research Letters*, *46*(14), 8517–8526. https://doi.org/10.1029/2019gl083699

Fromm, M., Bevilacqua, R., Servranckx, R., Rosen, J., Thayer, J. P., Herman, J., et al. (2005). Pyro-cumulonimbus injection of smoke to the stratosphere: Observations and impact of a super blowup in northwestern Canada on 3–4 August 1998. *Journal of Geophysical Research*, *110*(D8), D08205. https://doi.org/10.1029/2004jd005350

Fromm, M., Lindsey, D. T., Servranckx, R., Yue, G., Trickl, T., Sica, R., et al. (2010). The untold story of pyrocumulonimbus. *Bulletin of the American Meteorological Society*, *91*(9), 1193–1210. https://doi.org/10.1175/2010bams3004.1

Froyd, K. D., Murphy, D. M., Brock, C. A., Campuzano-Jost, P., Dibb, J. E., Jimenez, J. L., et al. (2019). A new method to quantify mineral dust and other aerosol species from aircraft platforms using single-particle mass spectrometry. *Atmospheric Measurement Techniques*, *12*(11), 6209–6239. https://doi.org/10.5194/amt-12-6209-2019

Hirsch, E., & Koren, I. (2021). Record-breaking aerosol levels explained by smoke injection into the stratosphere. *Science*, *371*(6535), 1269–1274. https://doi.org/10.1126/science.abe1415

Iacono, M. J., Delamere, J. S., Mlawer, E. J., Shephard, M. W., Clough, S. A., & Collins, W. D. (2008). Radiative forcing by long-lived greenhouse gases: Calculations with the AER radiative transfer models. *Journal of Geophysical Research*, *113*(D13), D13103. https://doi.org/10.1029/2008jd009944

Kablick, G. P., Allen, D. R., Fromm, M. D., & Nedoluha, G. E. (2020). Australian PyroCb smoke generates synoptic-scale stratospheric anticyclones. *Geophysical Research Letters*, *47*(13). https://doi.org/10.1029/2020gl088101

Khaykin, S., Legras, B., Bucci, S., Sellitto, P., Isaksen, L., Tencé, F., et al. (2020). The 2019/20 Australian wildfires generated a persistent smoke-charged vortex rising up to 35 km altitude. *Communications Earth & Environment*, *1*(1), 22. https://doi.org/10.1038/s43247-020-00022-5

Khaykin, S. M., Godin-Beekmann, S., Hauchecorne, A., Pelon, J., Ravetta, F., & Keckhut, P. (2018). Stratospheric smoke with unprecedentedly high backscatter observed by Lidars above southern France. *Geophysical Research Letters*, *45*(3), 1639–1646. https://doi.org/10.1002/2017gl076763

Kremser, S., Thomason, L. W., von Hobe, M., Hermann, M., Deshler, T., Timmreck, C., et al. (2016). Stratospheric aerosol—observations, processes, and impact on climate. *Reviews of Geophysics*, *54*(2), 278–335. https://doi.org/10.1002/2015rg000511

Lamarque, J. F., Emmons, L. K., Hess, P. G., Kinnison, D. E., Tilmes, S., Vitt, F., et al. (2012). CAM-chem: Description and evaluation of interactive atmospheric chemistry in the community Earth system model. *Geoscientific Model Development*, *5*(2), 369–411. https://doi.org/10.5194/gmd-5-369-2012

Larson, E. J. L., & Portmann, R. W. (2016). A temporal Kernel method to compute effective radiative forcing in CMIP5 transient simulations. *Journal of Climate*, *29*(4), 1497–1509. https://doi.org/10.1175/jcli-d-15-0577.1

Li, Y., Dykema, J., Deshler, T., & Keutsch, F. (2021). Composition dependence of stratospheric aerosol shortwave radiative forcing in Northern midlatitudes. *Geophysical Research Letters*, *48*(24), e2021GL094427. https://doi.org/10.1029/2021GL094427

Liu, X., Easter, R. C., Ghan, S. J., Zaveri, R., Rasch, P., Shi, X., et al. (2012). Toward a minimal representation of aerosols in climate models: Description and evaluation in the community atmosphere model CAM5. *Geoscientific Model Development*, *5*(3), 709–739. https://doi.org/10.5194/gmd-5-709-2012

Loughman, R., Bhartia, P. K., Chen, Z., Xu, P., Nyaku, E., & Taha, G. (2018). The ozone mapping and profiler suite (OMPS) Limb profiler (LP) version 1 aerosol extinction retrieval algorithm: Theoretical basis. *Atmospheric Measurement Techniques*, *11*(5), 2633–2651. https://doi.org/10.5194/amt-11-2633-2018

Mills, M. J., Schmidt, A., Easter, R., Solomon, S., Kinnison, D. E., Ghan, S. J., et al. (2016). Global volcanic aerosol properties derived from emissions, 1990–2014, using CESM1(WACCM). *Journal of Geophysical Research: Atmospheres*, *121*(5), 2332–2348. https://doi.org/10.1002/2015jd024290

Mlawer, E. J., Taubman, S. J., Brown, P. D., Iacono, M. J., & Clough, S. A. (1997). Radiative transfer for inhomogeneous atmospheres: RRTM, a validated correlated-k model for the longwave. *Journal of Geophysical Research*, *102*(D14), 16663–16682. https://doi.org/10.1029/97jd00237

Peterson, D. A., Campbell, J. R., Hyer, E. J., Fromm, M. D., Kablick, G. P., Cossuth, J. H., & DeLand, M. T. (2018). Wildfire-driven thunderstorms cause a volcano-like stratospheric injection of smoke. *npj Climate and Atmospheric Science*, *1*(1), 30. https://doi.org/10.1038/s41612-018-0039-3

Peterson, D. A., Fromm, M. D., McRae, R. H. D., Campbell, J. R., Hyer, E. J., Taha, G., et al. (2021). Australia's Black Summer pyrocumulonimbus super outbreak reveals potential for increasingly extreme stratospheric smoke events. *npj Climate and Atmospheric Science*, *4*(1), 38. https://doi.org/10.1038/s41612-021-00192-9

Ridley, D. A., Solomon, S., Barnes, J. E., Burlakov, V. D., Deshler, T., Dolgii, S. I., et al. (2014). Total volcanic stratospheric aerosol optical depths and implications for global climate change. *Geophysical Research Letters*, *41*(22), 7763–7769. https://doi.org/10.1002/2014gl061541

Rieger, L. A., Randel, W. J., Bourassa, A. E., & Solomon, S. (2021). Stratospheric temperature and ozone anomalies associated with the 2020 Australian New Year fires. *Geophysical Research Letters*, *48*(24). https://doi.org/10.1029/2021gl095898

Saleh, R., Robinson, E. S., Tkacik, D. S., Ahern, A. T., Liu, S., Aiken, A. C., et al. (2014). Brownness of organics in aerosols from biomass burning linked to their black carbon content. *Nature Geoscience*, *7*(9), 647–650. https://doi.org/10.1038/ngeo2220

Santee, M. L., Lambert, A., Manney, G. L., Livesey, N. J., Froidevaux, L., Neu, J. L., et al. (2022). Prolonged and pervasive perturbations in the composition of the southern Hemisphere midlatitude lower stratosphere from the Australian New Year's fires. *Geophysical Research Letters*, *49*(4), e2021GL096270. https://doi.org/10.1029/2021GL096270

Schmidt, A., Mills, M. J., Ghan, S., Gregory, J. M., Allan, R. P., Andrews, T., et al. (2018). Volcanic radiative forcing from 1979 to 2015. *Journal of Geophysical Research: Atmospheres*, *123*(22), 12491–12508. https://doi.org/10.1029/2018jd028776

Schmidt, G. A., Shindell, D. T., & Tsigaridis, K. (2014). Reconciling warming trends. *Nature Geoscience*, *7*(3), 158–160. https://doi.org/10.1038/ngeo2105

Sellitto, P., Belhadji, R., Kloss, C., & Legras, B. (2022). Radiative impacts of the Australian bushfires 2019–2020—Part 1: Large-scale radiative forcing. *Atmospheric Chemistry and Physics*, *22*(14), 9299–9311. https://doi.org/10.5194/acp-22-9299-2022

Smith, C. J., Kramer, R. J., Myhre, G., Forster, P. M., Soden, B. J., Andrews, T., et al. (2018). Understanding rapid adjustments to diverse forcing agents. *Geophysical Research Letters*, *45*(21), 12023–012031. https://doi.org/10.1029/2018GL079826

Solomon, S., Daniel, J. S., Neely, R. R., Vernier, J. P., Dutton, E. G., & Thomason, L. W. (2011). The persistently variable "background" stratospheric aerosol layer and global climate change. *Science*, *333*(6044), 866–870. https://doi.org/10.1126/science.1206027

Solomon, S., Dube, K., Stone, K., Yu, P., Kinnison, D., Toon, O. B., et al. (2022). On the stratospheric chemistry of midlatitude wildfire smoke. *Proceedings of the National Academy of Sciences*, *119*(10), e2117325119. https://doi.org/10.1073/pnas.2117325119

Stocker, M., Ladstädter, F., & Steiner, A. K. (2021). Observing the climate impact of large wildfires on stratospheric temperature. *Scientific Reports*, *11*(1), 22994. https://doi.org/10.1038/s41598-021-02335-7

Torres, O., Bhartia, P. K., Taha, G., Jethva, H., Das, S., Colarco, P., et al. (2020). Stratospheric injection of massive smoke plume from Canadian boreal fires in 2017 as seen by DSCOVR-EPIC, CALIOP, and OMPS-LP observations. *Journal of Geophysical Research: Atmospheres*, *125*(10). https://doi.org/10.1029/2020jd032579

Trickl, T., Giehl, H., Jäger, H., & Vogelmann, H. (2013). 35 yr of stratospheric aerosol measurements at garmisch-Partenkirchen: From Fuego to Eyjafjallajökull, and beyond. *Atmospheric Chemistry and Physics*, *13*(10), 5205–5225. https://doi.org/10.5194/acp-13-5205-2013

Yu, P., Davis, S. M., Toon, O. B., Portmann, R. W., Bardeen, C. G., Barnes, J. E., et al. (2021). Persistent stratospheric warming due to 2019-20 Australian wildfire smoke. *Geophysical Research Letters*, *48*(7). https://doi.org/10.1029/2021gl092609

Yu, P., Toon, O. B., Bardeen, C. G., Zhu, Y., Rosenlof, K. H., Portmann, R. W., et al. (2019). Black carbon lofts wildfire smoke high into the stratosphere to form a persistent plume. *Science*, *365*(6453), 587–590. https://doi.org/10.1126/science.aax1748

References From the Supporting Information

Andersson, S. M., Martinsson, B. G., Vernier, J.-P., Friberg, J., Brenninkmeijer, C. A. M., Hermann, M., et al. (2015). Significant radiative impact of volcanic aerosol in the lowermost stratosphere. *Nature Communications*, *6*(1), 7692. https://doi.org/10.1038/ncomms8692

Froyd, K. D., Yu, P., Schill, G. P., Brock, C. A., Kupc, A., Williamson, C. J., et al. (2022). Dominant role of mineral dust in cirrus cloud formation revealed by global-scale measurements. *Nature Geoscience*, *15*(3), 177–183. https://doi.org/10.1038/s41561-022-00901-w

Hess, M., Koepke, P., & Schult, I. (1998). Optical properties of aerosols and clouds: The software package OPAC. *Bulletin of the American Meteorological Society*, *79*(5), 831–844. https://doi.org/10.1175/1520-0477(1998)079<0831:Opoaac>2.0.Co;2

Hurrell, J. W., Hack, J. J., Shea, D., Caron, J. M., & Rosinski, J. (2008). A New sea surface temperature and sea ice boundary dataset for the community atmosphere model. *Journal of Climate*, *21*(19), 5145–5153. https://doi.org/10.1175/2008jcli2292.1

Knepp, T. N., Thomason, L., Roell, M., Damadeo, R., Leavor, K., Leblanc, T., et al. (2020). Evaluation of a method for converting Stratospheric Aerosol and Gas Experiment (SAGE) extinction coefficients to backscatter coefficients for intercomparison with lidar observations. *Atmospheric Measurement Techniques*, *13*(8), 4261–4276. https://doi.org/10.5194/amt-13-4261-2020

Yu, P., Froyd, K. D., Portmann, R. W., Toon, O. B., Freitas, S. R., Bardeen, C. G., et al. (2019a). Efficient in-cloud removal of aerosols by deep convection. *Geophysical Research Letters*, *46*(2), 1061–1069. https://doi.org/10.1029/2018gl080544

Yu, P., Toon, O. B., Bardeen, C. G., Mills, M. J., Fan, T., English, J. M., & Neely, R. R. (2015). Evaluations of tropospheric aerosol properties simulated by the community Earth system model with a sectional aerosol microphysics scheme. *Journal of Advances in Modeling Earth Systems*, *7*(2), 865–914. https://doi.org/10.1002/2014MS000421